Appl. Math. Mech. -Engl. Ed., **41**(7), 1011–1026 (2020)

APPLIED MATHEMATICS AND MECHANICS (ENGLISH EDITION)

https://doi.org/10.1007/s10483-020-2631-7

Influence of elastic foundations and carbon nanotube reinforcement on the hydrostatic buckling pressure of truncated conical shells*

A. H. SOFIYEV[1,2,†], I. T. PIRMAMEDOV[2], N. KURUOGLU[3]

1. Department of Civil Engineering, Suleyman Demirel University, Isparta 32260, Turkey;
2. Department of Mathematics, Azerbaijan Technical University, Baku 1073, Azerbaijan;
3. Department of Civil Engineering, Gelisim University, Istanbul 34310, Turkey

(Received Feb. 21, 2020 / Revised Apr. 15, 2020)

Abstract In this study, the effects of elastic foundations (EFs) and carbon nanotube (CNT) reinforcement on the hydrostatic buckling pressure (HBP) of truncated conical shells (TCSs) are investigated. The first order shear deformation theory (FOSDT) is generalized to the buckling problem of TCSs reinforced with CNTs resting on the EFs for the first time. The material properties of composite TCSs reinforced with CNTs are graded linearly according to the thickness coordinate. The Winkler elastic foundation (W-EF) and Pasternak elastic foundation (P-EF) are considered as the EF. The basic relations and equations of TCSs reinforced with CNTs on the EFs are obtained in the framework of the FOSDT and solved using the Galerkin method. One of the innovations in this study is to obtain a closed-form solution for the HBP of TCSs reinforced with CNTs on the EFs. Finally, the effects of the EFs and various types CNT reinforcements on the HBP are investigated simultaneously. The obtained results are compared with the results in the literature, and the accuracy of results is confirmed.

Key words truncated conical shell (TCS), carbon nanotube (CNT), Winkler elastic foundation (W-EF), Pasternak elastic foundation (P-EF), hydrostatic pressure, buckling

Chinese Library Classification O310
2010 Mathematics Subject Classification 74K25, 74M25, 74G10

1 Introduction

Since carbon nanotubes (CNTs) are flexible, durable, and powerful, it is becoming more and more attractive for use as a reinforcing element in various fields of technology[1–3]. Structural elements reinforced by nanotubes are lighter, stronger, and more resistant to heat and radiation, and are often used in various areas of the spacecraft, defense industry, and mechanical engineering. Since structural elements reinforced with CNTs have become inevitable in various environments, it is very important to determine the influence of elastic media on their behavior during design. Many foundation models have been proposed to better describe the structure of soils. The simplest model for an elastic foundation (EF) is the Winkler model, it was later

* Citation: SOFIYEV, A. H., PIRMAMEDOV, I. T., and KURUOGLU, N. Influence of elastic foundations and carbon nanotube reinforcement on the hydrostatic buckling pressure of truncated conical shells. *Applied Mathematics and Mechanics* (*English Edition*), **41**(7), 1011–1026 (2020) https://doi.org/10.1007/s10483-020-2631-7

† Corresponding author, E-mail: abdullahavey@sdu.edu.tr

developed by Pasternak, which takes into account the interaction of springs separated in the Winkler model by adding a new dependent parameter[4]. Since then, the Pasternak model has been widely used to describe the mechanical behavior of structures that interact with the EFs. The basic information on these models and their interaction problems with the structural elements are presented in detail in Refs. [5]–[7]. A study on the behavior of truncated conical shells (TCSs) on the Pasternak elastic foundation (P-EF) is first found in Ref. [8].

Thus, in recent years, researchers began to study analyzes of the bending, buckling, and vibration of structural elements reinforced with CNTs on the EFs. One of the first studies on the buckling of shell structures reinforced with CNTs resting on the EFs belongs to Shen and Xiang[9]. After this work, a number of studies were carried out, most of which belonged to Shen and co-authors[10–13], as well as the work of Bidgoli et al.[14] and Mohammadi et al.[15] have been published. At the same time, the problems of bending, buckling, and vibration of plates reinforced with CNTs on the EFs have been studied since 2015, which continue to this day[16–27].

The literature review by the authors reveals that the number of studies for buckling and vibration of TCSs reinforced with CNTs on the EFs is rather limited compared with plates and cylindrical shells reinforced with CNTs. One of these studies was described by Duc et al.[28], the authors addressed the solution of the stability of TCSs reinforced with CNTs under the axial load and resting on the EFs. Thanh et al.[29] studied dynamic response and vibration of TCSs reinforced with CNTs and resting on the EFs. In the above studies[28–29], the stability and vibration of TCSs have been addressed in the framework of the classical shell theory (CST).

As far as the authors know, there is no literature describing the buckling of TCSs reinforced with CNTs and resting on the EFs based on the first order shear deformation theory (FOSDT). The FOSDT is generalized to the buckling problem of TCSs reinforced with CNTs resting on the EFs for the first time. One of the unique aspects of this study is that shear stress functions are used for TCSs reinforced with CNTs instead of the shear correction factor. The influences of shear strains are included in the fundamental relations and basic equations in the form of parabolic functions. One of the innovations in this study is to obtain formula for the hydrostatic buckling pressure (HBP) of TCSs reinforced with CNTs on the EFs within the FOSDT. Finally, numerical calculations are performed to show the influences of EFs on the HBP for the TCSs reinforced with CNTs for different volume fractions and geometries.

2 Multi-scale model for TCSs reinforced with CNTs

Let us assume that the TCS reinforced with CNTs on the EFs is exposed to the uniform hydrostatic pressure, $T_{\rm H}$ (see Fig. 1). The length, small and large radii, thickness and semi-vertex angle of the TCS are l, r_1, r_2, h, and θ, respectively. In this case, the membrane forces $N_{x0}, N_{\varphi 0}$, and $N_{x\varphi 0}$ for the condition with zero initial moments are determined as follows:

$$\begin{cases} N_{x0} = -0.5T_{\rm H}\dfrac{x}{\cot\theta}, \\ N_{\varphi 0} = -T_{\rm H}\dfrac{x}{\cot\theta}, \\ N_{x\varphi 0} = 0. \end{cases} \tag{1}$$

Let us assume that the origin of the coordinate system $Ox\varphi\zeta$ is chosen so that it is at the top of the cone, on the reference surface of the shell. Let u, v, and w be the cone displacements parallel to a right hand set of axes (x, φ, ζ), in which x is longitudinal, φ is circumferential, and ζ is perpendicular to the shell surface, and ψ_1 and ψ_2 are the mid-surface rotations of the normal about the φ- and x-axes, respectively. The conical shell resting on the P-EF and the reaction force per unit area, N_0 of the P-EF to TCSs is formulated as follows[3–8]:

$$N_0 = k_1 w - k_2 \nabla^2 w, \tag{2}$$

where k_1 is the Winkler spring stiffness (N/m^3), k_2 is shearing layer stiffness of the foundation (N/m), $\varphi_0 = \varphi \sin\theta$, and $\nabla^2 w = (w_{,xx} + w_{,x}/x + w_{,\varphi_0\varphi_0}/x^2)$ is Laplace operator for x and φ[8]. Here, a coma denotes partial differentiation versus the coordinates. When $k_2 = 0$, the P-EF turns into the Winkler elastic foundation (W-EF).

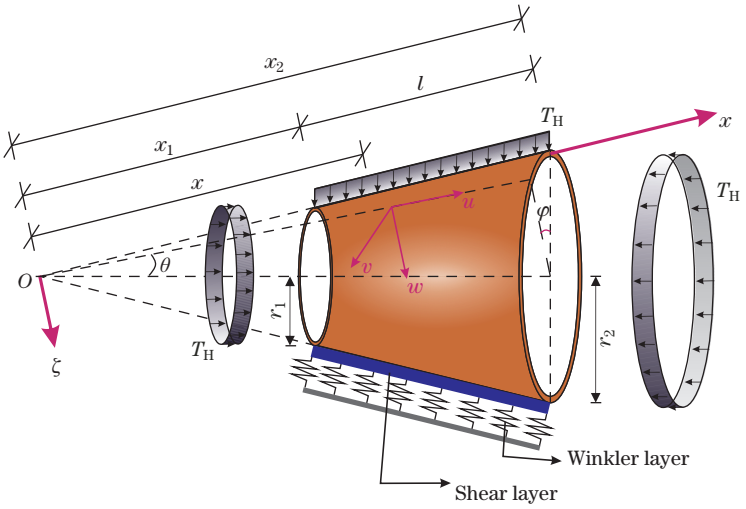

Fig. 1 TCS reinforced with CNTs under the hydrostatic pressure on the P-EF and notations (color online)

When the stress function is expressed by Ψ, the relationship between the force components (N_x, N_φ, $N_{x\varphi}$) will be[30]

$$(N_x,\, N_\varphi,\, N_{x\varphi}) = \Big(\frac{1}{x^2}\frac{\partial^2\Psi}{\partial\varphi_0^2} + \frac{1}{x}\frac{\partial\Psi}{\partial x},\, \frac{\partial^2\Psi}{\partial x^2},\, -\frac{1}{x}\frac{\partial^2\Psi}{\partial x\partial\varphi_0} + \frac{1}{x^2}\frac{\partial\Psi}{\partial\varphi_0}\Big)h. \tag{3}$$

The FOSDT was developed by Ambartsumian[30], who assumed the parabolic distributions of the transverse shear strains over the thickness of the shells. One of the advantages of this theory is that the number of independent unknowns is four $(\Psi, w, \psi_1, \psi_2)$, and the shear correction factor is not used. On the basis of the FOSDT, the basic equations for TCSs reinforced with CNTs on the P-EF can be derived in terms of Ψ, w, ψ_1, and ψ_2 as

$$\begin{cases} L_{11}(\Psi) + L_{12}(w) + L_{13}(\psi_1) + L_{14}(\psi_2) = 0, \\ L_{21}(\Psi) + L_{22}(w) + L_{23}(\psi_1) + L_{24}(\psi_2) = 0, \\ L_{31}(\Psi) + L_{32}(w) + L_{33}(\psi_1) + L_{34}(\psi_2) = 0, \\ L_{41}(\Psi) + L_{42}(w) + L_{43}(\psi_1) + L_{44}(\psi_2) - k_1 w + k_2\nabla^2 w = 0, \end{cases} \tag{4}$$

where $L_{ij}(i,j=1,2,3,4)$ are differential operators and defined as

$$\begin{cases} L_{11}=h\Big(a_{12}\dfrac{\partial^4}{\partial x^4}+\dfrac{a_{11}-a_{31}}{x^2}\dfrac{\partial^4}{\partial x^2\partial\phi_0^2}+\dfrac{3a_{31}-a_{21}-3a_{11}}{x^3}\dfrac{\partial^3}{\partial x\partial\phi_0^2}+\dfrac{a_{11}+a_{12}-a_{22}}{x}\dfrac{\partial^3}{\partial x^3}\\ \qquad +\dfrac{a_{22}-a_{12}-a_{11}-a_{21}}{x^2}\dfrac{\partial^2}{\partial x^2}+\dfrac{3\left(a_{21}+a_{11}-a_{31}\right)}{x^4}\dfrac{\partial^2}{\partial\phi_0^2}+\dfrac{2a_{21}}{x^3}\dfrac{\partial}{\partial x}\Big),\\ L_{12}=-a_{13}\dfrac{\partial^4}{\partial x^4}-\dfrac{a_{14}+a_{32}}{x^2}\dfrac{\partial^4}{\partial x^2\partial\phi_0^2}+\dfrac{3a_{14}+3a_{32}+a_{24}}{x^3}\dfrac{\partial^3}{\partial x\partial\phi_0^2}-\dfrac{a_{13}+a_{14}-a_{23}}{x}\dfrac{\partial^3}{\partial x^3}\\ \qquad +\dfrac{a_{13}+a_{14}-a_{23}+a_{24}}{x^2}\dfrac{\partial^2}{\partial x^2}-\dfrac{3(a_{14}+a_{24}+a_{32})}{x^4}\dfrac{\partial^2}{\partial\phi_0^2}-\dfrac{2a_{24}}{x^3}\dfrac{\partial}{\partial x},\\ L_{13}=a_{15}\dfrac{\partial^3}{\partial x^3}+\dfrac{a_{15}-a_{25}}{x}\dfrac{\partial^2}{\partial x^2}+\dfrac{a_{35}}{x^2}\dfrac{\partial^3}{\partial x\partial\phi_0^2}-t_3\dfrac{\partial}{\partial x}-\dfrac{a_{15}-a_{25}}{x^2}\dfrac{\partial}{\partial x}-\dfrac{a_{35}}{x^3}\dfrac{\partial^2}{\partial\phi_0^2},\\ L_{14}=\dfrac{a_{38}+a_{18}}{x}\dfrac{\partial^3}{\partial x^2\partial\phi_0}-\dfrac{a_{28}+a_{18}+a_{38}}{x^2}\dfrac{\partial^2}{\partial x\partial\phi_0}+\dfrac{2a_{28}}{x^3}\dfrac{\partial}{\partial\phi_0}, \end{cases} \tag{5a}$$

$$\begin{cases} L_{21}=h\Big(\dfrac{a_{21}h}{x^3}\dfrac{\partial^4}{\partial\phi_0^4}+\dfrac{(a_{22}-a_{31})}{x}\dfrac{\partial^4}{\partial x^2\partial\phi_0^2}+\dfrac{a_{21}}{x^2}\dfrac{\partial^3}{\partial x\partial\phi_0^2}\Big),\\ L_{22}=-\dfrac{a_{32}+a_{23}}{x}\dfrac{\partial^4}{\partial x^2\partial\phi_0^2}-\dfrac{a_{24}}{x^2}\dfrac{\partial^3}{\partial x\partial\phi_0^2}-\dfrac{a_{24}}{x^3}\dfrac{\partial^4}{\partial\phi_0^4},\\ L_{23}=\dfrac{a_{25}+a_{35}}{x}\dfrac{\partial^3}{\partial x\partial\phi_0^2}+\dfrac{a_{35}}{x^2}\dfrac{\partial^2}{\partial\phi_0^2},\\ L_{24}=a_{38}\dfrac{\partial^3}{\partial x^2\partial\phi_0}+\dfrac{2a_{38}}{x}\dfrac{\partial^2}{\partial x\partial\phi_0}+\dfrac{a_{28}}{x^2}\dfrac{\partial^3\psi}{\partial\phi_0^3}-t_4\dfrac{\partial}{\partial\phi_0}, \end{cases} \tag{5b}$$

$$\begin{cases} L_{31}=h\Big(\dfrac{\vartheta_{11}}{x^4}\dfrac{\partial^4}{\partial\phi_0^4}+\dfrac{(2\vartheta_{31}+\vartheta_{21}+\vartheta_{12})}{x^2}\dfrac{\partial^4}{\partial x^2\partial\phi_0^2}-\dfrac{2(\vartheta_{31}+\vartheta_{21})}{x^3}\dfrac{\partial^3}{\partial x\partial\phi_0^2}\\ \qquad +\dfrac{2(\vartheta_{31}+\vartheta_{21}+\vartheta_{11})}{x^4}\dfrac{\partial^2}{\partial\phi_0^2}+\dfrac{\vartheta_{11}}{x^3}\dfrac{\partial}{\partial x}-\dfrac{\vartheta_{11}}{x^2}\dfrac{\partial^2}{\partial x^2}+\dfrac{(\vartheta_{21}+2\vartheta_{22}-\vartheta_{12})}{x}\dfrac{\partial^3}{\partial x^3}+\vartheta_{22}\dfrac{\partial^4}{\partial x^4}\Big),\\ L_{32}=-\dfrac{\vartheta_{14}}{x^4}\dfrac{\partial^4}{\partial\phi_0^4}+\dfrac{2\vartheta_{32}-\vartheta_{13}-\vartheta_{24}}{x^2}\dfrac{\partial^4}{\partial x^2\partial\phi_0^2}+\dfrac{2(\vartheta_{24}-\vartheta_{32})}{x^3}\dfrac{\partial^3}{\partial x\partial\phi_0^2}\\ \qquad +\dfrac{2(\vartheta_{32}-\vartheta_{24}-\vartheta_{14})}{x^4}\dfrac{\partial^2}{\partial\phi_0^2}-\dfrac{\vartheta_{14}}{x^3}\dfrac{\partial}{\partial x}+\left(\dfrac{\vartheta_{14}}{x^2}+\dfrac{\cot\theta}{x}\right)\dfrac{\partial^2}{\partial x^2}\\ \qquad +\dfrac{\vartheta_{13}-\vartheta_{24}-2\vartheta_{23}}{x}\dfrac{\partial^3}{\partial x^3}-\vartheta_{23}\dfrac{\partial^4}{\partial x^4},\\ L_{33}=\dfrac{2\vartheta_{35}+\vartheta_{15}}{x^2}\dfrac{\partial^3}{\partial x\partial\phi_0^2}+\vartheta_{25}\dfrac{\partial^3}{\partial x^3}+\dfrac{2\vartheta_{25}-\vartheta_{15}}{x}\dfrac{\partial^2}{\partial x^2},\\ L_{34}=\dfrac{\vartheta_{18}}{x^3}\dfrac{\partial^3}{\partial\phi_0^3}+\dfrac{2\vartheta_{38}+\vartheta_{28}}{x}\dfrac{\partial^3}{\partial x^2\partial\phi_0}+\dfrac{2\vartheta_{38}-\vartheta_{18}}{x^2}\dfrac{\partial^2}{\partial x\partial\phi_0}+\dfrac{\vartheta_{18}}{x^3}\dfrac{\partial}{\partial\phi_0}, \end{cases} \tag{5c}$$

$$\begin{cases} L_{41}=\dfrac{h\cot\theta}{x}\dfrac{\partial^2}{\partial x^2},\\ L_{42}=-\dfrac{T_Hx}{\cot\theta}\dfrac{\partial^2}{\partial x^2}-\dfrac{T_Hx}{\cot\theta}\left(\dfrac{1}{x}\dfrac{\partial^2}{\partial\phi_0^2}+\dfrac{\partial}{\partial x}\right)-k_1+k_2\left(\dfrac{\partial^2}{\partial x^2}+\dfrac{1}{x}\dfrac{\partial}{\partial x}+\dfrac{1}{x^2}\dfrac{\partial^2}{\partial\phi_0^2}\right),\\ L_{43}=t_3\left(\dfrac{\partial}{\partial x}+\dfrac{1}{x}\right),\quad L_{44}=\dfrac{t_4}{x}\dfrac{\partial}{\partial\phi_0}, \end{cases} \tag{5d}$$

in which $t_3 = t_4 = f(0.5h) - f(-0.5h)$, and the following definitions are used:

$$\begin{cases} a_{11} = A_{11}^1\vartheta_{11} + A_{12}^1\vartheta_{21}, \quad a_{12} = A_{11}^1\vartheta_{12} + A_{12}^1\vartheta_{21}, \\ a_{13} = A_{11}^1\vartheta_{13} + A_{12}^1\vartheta_{23} + A_{11}^2, \quad a_{14} = A_{11}^1\vartheta_{14} + A_{12}^1\vartheta_{24} + A_{12}^2, \\ a_{15} = A_{11}^1\vartheta_{15} + A_{12}^1\vartheta_{25} + A_{15}^1, \quad a_{18} = A_{11}^1\vartheta_{18} + A_{12}^1\vartheta_{28} + A_{18}^1, \\ a_{21} = A_{11}^1\vartheta_{11} + A_{22}^1\vartheta_{21}, \quad a_{22} = A_{22}^1\vartheta_{12} + A_{21}^1\vartheta_{22}, \\ a_{23} = A_{21}^1\vartheta_{13} + A_{22}^1\vartheta_{23} + A_{21}^2, \quad a_{24} = A_{21}^1\vartheta_{14} + A_{22}^1\vartheta_{24} + A_{22}^2, \\ a_{25} = A_{21}^1\vartheta_{15} + A_{22}^1\vartheta_{25} + A_{25}^1, \quad a_{28} = A_{21}^1\vartheta_{18} + A_{22}^1\vartheta_{28} + A_{28}^1, \\ a_{31} = A_{66}^1\vartheta_{31}, \quad a_{32} = A_{66}^1\vartheta_{32} + 2A_{66}^2, \\ a_{35} = A_{35}^1 - A_{66}^1\vartheta_{35}, \quad a_{38} = A_{38}^1 - A_{66}^1\vartheta_{38}, \\ \vartheta_{11} = A_{22}^0 u, \quad \vartheta_{12} = -A_{12}^0\upsilon, \\ \vartheta_{13} = \left(A_{12}^0A_{21}^1 - A_{11}^0A_{22}^0\right)\upsilon, \quad \vartheta_{14} = \left(A_{12}^0A_{21}^1 - A_{12}^1A_{22}^0\right)\upsilon, \\ \vartheta_{15} = \left(A_{25}^0A_{12}^0 - A_{15}^0A_{22}^0\right)\upsilon, \quad \vartheta_{18} = \left(A_{28}^0A_{12}^0 - A_{18}^0A_{22}^0\right)\upsilon, \\ \vartheta_{21} = -A_{21}^0 u, \quad \vartheta_{22} = A_{11}^0\upsilon, \quad \vartheta_{23} = \left(A_{11}^1A_{21}^0 - A_{21}^1A_{11}^0\right)\upsilon, \\ \vartheta_{24} = \left(A_{12}^1A_{21}^0 - A_{21}^1A_{11}^0\right)\upsilon, \quad \vartheta_{25} = \left(A_{15}^0A_{21}^0 - A_{25}^0A_{11}^0\right)\upsilon, \\ \vartheta_{28} = \left(A_{18}^0A_{21}^0 - A_{28}^0A_{11}^0\right)\upsilon, \quad \upsilon = \left(A_{11}^0A_{22}^0 - A_{12}^0A_{21}^0\right)^{-1}, \\ \vartheta_{31} = 1/A_{66}^0, \quad \vartheta_{32} = -2A_{66}^1/A_{66}^0, \\ \vartheta_{35} = A_{35}^0/A_{66}^0, \quad \vartheta_{38} = A_{38}^0/A_{66}^0, \end{cases} \tag{6}$$

where

$$\begin{cases} A_{11}^i = \displaystyle\int_{-0.5h}^{0.5h} q_{11}\zeta^i \mathrm{d}\zeta, \quad A_{12}^i = \int_{-0.5h}^{0.5h} q_{12}\zeta^i \mathrm{d}\zeta = \int_{-0.5h}^{0.5h} q_{21}\zeta^i \mathrm{d}\zeta = A_{21}^i, \\ A_{22}^i = \displaystyle\int_{-0.5h}^{0.5h} q_{22}\zeta^i \mathrm{d}\zeta, \quad A_{66}^i = \int_{-0.5h}^{0.5h} q_{66}\zeta^i \mathrm{d}\zeta, \quad i = 0, 1, 2, \\ A_{15}^j = \displaystyle\int_{-0.5h}^{0.5h} \zeta^j t_1 q_{11} \mathrm{d}\zeta, \quad A_{18}^j = \int_{-0.5h}^{0.5h} \zeta^j t_2 q_{12} \mathrm{d}\zeta, \\ A_{25}^j = \displaystyle\int_{-0.5h}^{0.5h} \zeta^j t_1 q_{21} \mathrm{d}\zeta, \quad A_{28}^j = \int_{-0.5h}^{0.5h} \zeta^j t_2 A_{22} \mathrm{d}\zeta, \\ A_{35}^j = \displaystyle\int_{-0.5h}^{0.5h} \zeta^j t_1 q_{66} \mathrm{d}\zeta, \quad A_{38}^j = \int_{-0.5h}^{0.5h} \zeta^j t_2 q_{66} \mathrm{d}\zeta, \quad j = 0, 1. \end{cases} \tag{7}$$

In the above equations, the forces (N_{ij}, Q_i) and moments (M_{ij}) are defined as[30–32]

$$(N_{ij}, Q_i,\ M_{ij}) = \int_{-0.5h}^{0.5h} (\sigma_{ij}, \sigma_{iz}, \zeta\sigma_{ij})\, \mathrm{d}\zeta, \quad i, j = x, \varphi, \tag{8}$$

where $\sigma_{ij}(i, j = x, \varphi, \zeta)$ are the stress components of TCSs reinforced with CNTs.

In order to extend the FOSDT to the TCSs reinforced with CNTs, it is necessary to evaluate equivalent material properties that usually take into account the influence of nanotubes with multi-scale modeling of CNTs and matrices.

According to the extended mixing rule, the effective Young's modulus (Y_{ij}) and shear modulus (S_{ij}) of TCSs reinforced with CNTs can be expressed as follows[9]:

$$\begin{cases} Y_{11} = e_1 V_{\mathrm{cn}} Y_{11}^{\mathrm{cn}} + V_{\mathrm{m}} Y^{\mathrm{m}}, \quad \dfrac{e_2}{Y_{22}} = \dfrac{V_{\mathrm{cn}}}{Y_{22}^{\mathrm{cn}}} + \dfrac{V_{\mathrm{m}}}{Y^{\mathrm{m}}}, \\ \dfrac{e_3}{S_{12}} = \dfrac{V_{\mathrm{cn}}}{S_{12}^{\mathrm{cn}}} + \dfrac{V_{\mathrm{m}}}{S^{\mathrm{m}}}, \quad S_{13} = S_{12}, \quad S_{23} = 1.2S_{12}, \end{cases} \tag{9}$$

where Young's and shear moduli of the CNTs and matrix are denoted by $Y_{11}^{\rm cn}, Y_{22}^{\rm cn}$, $S_{12}^{\rm cn}$, $Y^{\rm m}$, and $S^{\rm m}$, respectively, the volume fraction of TCSs reinforced with CNTs and efficiency parameters of CNTs are denoted by $V_{\rm cn}$ and e_j $(j=1,2,3)$, respectively. $V_{\rm m}$ is the volume fraction of the matrix, which satisfies the relationship of $V_{\rm cn}+V_{\rm m}=1$.

As already mentioned, the load transfer between the nanotube and the polymer phase due to a number of effects, such as effects of the surface, the strain gradient, and the intermolecular coupled stress, is not ideal. Therefore, in order to consider the small-scale effect and other effects on the material properties of TCSs reinforced with CNTs, we introduce the CNT efficiency parameter e_j $(j=1,2,3)$ in formula (9).

Since the change of the Poisson's ratio (p) of TCSs reinforced with CNTs along the thickness coordinate is weak (insignificant), the following relation is used for p_{12}:

$$p_{12}=V_{\rm cn}^{*}p_{\rm cn}^{12}+V_{\rm m}p^{\rm m}, \tag{10}$$

where $V_{\rm cn}^{*}$ is the volume fraction of CNTs and defined as[9]

$$V_{\rm cn}^{*}=\frac{m_{\rm cn}}{m_{\rm cn}+(d^{\rm cn}/d^{\rm m})-(d^{\rm cn}/d^{\rm m})m_{\rm cn}}, \tag{11}$$

where $m_{\rm cn}$ is the mass fraction of CNTs, $d^{\rm cn}$ and $d^{\rm m}$ are densities of the CNT and matrix, respectively.

In accordance with the FOSDT, the matrix relationship is formed between the stress and strain components of TCSs reinforced with CNTs as

$$\begin{bmatrix}\sigma_{xx}\\ \sigma_{\varphi\varphi}\\ \sigma_{xz}\\ \sigma_{\varphi z}\\ \sigma_{x\varphi}\end{bmatrix}=\begin{bmatrix}q_{11}&q_{12}&0&0&0\\ q_{21}&q_{22}&0&0&0\\ 0&0&q_{44}&0&0\\ 0&0&0&q_{55}&0\\ 0&0&0&0&q_{66}\end{bmatrix}\begin{bmatrix}e_{xx}\\ e_{\varphi\varphi}\\ \gamma_{xz}\\ \gamma_{\varphi z}\\ \gamma_{x\varphi}\end{bmatrix}, \tag{12}$$

where e_{ii} $(i=x,\varphi)$ and γ_{ij} $(i,j=x,\varphi,z)$ are normal and shear strains, and the definition of q_{ij} $(i,j=1,2,6)$ is presented below:

$$\begin{cases} q_{11}=\dfrac{Y_{11}(\overline{\zeta})}{1-p_{12}p_{21}}, \quad q_{22}=\dfrac{Y_{22}(\overline{\zeta})}{1-p_{12}p_{21}},\\ q_{12}=\dfrac{p_{21}Y_{11}(\overline{\zeta})}{1-p_{12}p_{21}}=\dfrac{p_{12}Y_{22}(\overline{\zeta})}{1-p_{12}p_{21}}=q_{21},\\ q_{44}=Y_{23}(\overline{\zeta}), \quad q_{55}=Y_{13}(\overline{\zeta}), \quad q_{66}=Y_{12}(\overline{\zeta}). \end{cases} \tag{13}$$

In accordance with the FOSDT, since the shear stresses $\sigma_{x\zeta}$ and $\sigma_{\varphi\zeta}$ for the TCSs reinforced with CNTs are assumed to vary depending on the thickness coordinate, they are expressed as follows[30]:

$$\sigma_{x\zeta}=f_{,\zeta}\,\psi_1, \quad \sigma_{\varphi\zeta}=f_{,\zeta}\,\psi_2, \tag{14}$$

where $f(\zeta)$ is the posteriori specified shape function, which defined as $f(\zeta)=\zeta-4\zeta^3/(3h^2)$.

Unlike the CST, since the displacements in the x- and φ-directions of any point at a distance ζ from the mid-surface of TCSs reinforced with CNTs within FOSDT are not linearly related to the ζ coordinate, as a rule, the following expressions for strains on the mid-surface (e_{xx},

$e_{\varphi\varphi}, \gamma_{0x\varphi}$) are obtained:

$$\begin{bmatrix} e_{xx} \\ e_{\varphi\varphi} \\ \gamma_{x\varphi} \end{bmatrix} = \begin{bmatrix} \varepsilon_{xx} - \zeta\dfrac{\partial^2 w}{\partial x^2} + t_1\dfrac{\partial\psi_1}{\partial x} \\ \varepsilon_{\varphi\varphi} - \zeta\Big(\dfrac{1}{x^2}\dfrac{\partial^2 w}{\partial\varphi_0^2} + \dfrac{1}{x}\dfrac{\partial w}{\partial x}\Big) + t_2\dfrac{1}{x}\dfrac{\partial\psi_2}{\partial\varphi_0} \\ \gamma_{0x\varphi} - 2\zeta\Big(\dfrac{1}{x}\dfrac{\partial^2 w}{\partial x\partial\varphi_0} - \dfrac{1}{x^2}\dfrac{\partial w}{\partial\varphi_0}\Big) + t_1\dfrac{1}{x}\dfrac{\partial\psi_1}{\partial\varphi_0} + t_2\dfrac{\partial\psi_2}{\partial x} \end{bmatrix}, \tag{15}$$

where $\varphi_0 = \varphi\sin\theta$, and the following definitions are used:

$$t_1 = \int_0^\zeta f_{,\zeta}\, q_{55}^{-1}\mathrm{d}\zeta, \quad t_2 = \int_0^\zeta f_{,\zeta}\, q_{44}^{-1}\mathrm{d}\zeta. \tag{16}$$

3 Solution to governing equations

Since the TCSs reinforced with CNTs are subjected to freely-supported (F-S) boundary conditions from the edges, the following approximation functions are used to solve basic equations[33]:

$$\begin{cases} \Psi = \Psi_0 x_2 \mathrm{e}^{(\eta+1)\overline{x}}\sin(\delta_1\overline{x})\cos(\delta_2\varphi_0), \quad w = w_0\mathrm{e}^{\eta\overline{x}}\sin(\delta_1\overline{x})\cos(\delta_2\varphi_0), \\ \psi_1 = \Psi_1\mathrm{e}^{\eta\overline{x}}\cos(\delta_1\overline{x})\cos(\delta_2\varphi_0), \quad \psi_2 = \Psi_2\mathrm{e}^{\eta\overline{x}}\sin(\delta_1\overline{x})\sin(\delta_2\varphi_0), \end{cases} \tag{17}$$

where Ψ_0, w_0, Ψ_1, and Ψ_2 are amplitudes, η is an unknown parameter to be found from the minimum conditions of the HBP, $\overline{x} = \ln\big(\frac{x}{x_2}\big)$, $\delta_1 = \frac{m\pi}{x_0}$, $\delta_2 = \frac{n}{\sin\theta}$, $x_0 = \ln\big(\frac{x_2}{x_1}\big)$, in which m and n are the wave numbers.

After substituting Eq. (17) into Eq. (4) and applying the Galerkin method, after some transformation, the matrix equations are obtained as follows:

$$\begin{bmatrix} s_{11} & -s_{12} & s_{13} & s_{14} \\ s_{21} & -s_{22} & s_{23} & s_{24} \\ s_{31} & -s_{32} & s_{33} & s_{34} \\ s_{41} & s_{42} & s_{43} & s_{44} \end{bmatrix} \begin{bmatrix} \Psi_0 \\ w_0 \\ \Psi_1 \\ \Psi_2 \end{bmatrix} = \begin{bmatrix} 0 \\ 0 \\ 0 \\ 0 \end{bmatrix}, \tag{18}$$

where s_{ij} $(i, j = 1, 2, 3, 4)$ are parameters depending on the TCSs reinforced with CNTs[33].

To find a nontrivial solution of Eq. (18), the determinant of the matrix of the left-hand side is equal to zero, and after some mathematical operations, an analytical expression is found for the dimensionless hydrostatic buckling pressure (DHBP) of TCSs reinforced with CNTs on the P-EF in the framework of the FOSDT:

$$\begin{aligned} T_{1\mathrm{sdt}}^{\mathrm{crwp}} =& \frac{1}{s_{T_\mathrm{H}} Y^\mathrm{m}} \\ & \cdot\Big(\frac{(\lambda_4 - \frac{\lambda_1\lambda_6}{\lambda_3})(\lambda_8 - \frac{\lambda_2\lambda_6}{\lambda_3}) - (\lambda_5 - \frac{\lambda_2\lambda_6}{\lambda_3})(\lambda_7 - \frac{\lambda_1\lambda_9}{\lambda_3})}{(\lambda_4 - \frac{\lambda_1\lambda_6}{\lambda_3})} + k_\mathrm{w}s_{k_\mathrm{w}} + k_\mathrm{p}s_{k_\mathrm{p}}\Big), \end{aligned} \tag{19}$$

where

$$\begin{cases} \lambda_1 = \dfrac{s_{21}s_{14} - s_{11}s_{24}}{s_{14}}, & \lambda_2 = \dfrac{s_{12}s_{24} - s_{22}s_{14}}{s_{14}}, & \lambda_3 = \dfrac{s_{23}s_{14} - s_{24}s_{13}}{s_{14}}, \\ \lambda_4 = \dfrac{s_{31}s_{14} - s_{11}s_{34}}{s_{14}}, & \lambda_5 = \dfrac{s_{12}s_{34} - s_{32}s_{14}}{s_{14}}, & \lambda_6 = \dfrac{s_{33}s_{14} - s_{13}s_{34}}{s_{14}}, \\ \lambda_7 = \dfrac{s_{41}s_{14} - s_{11}s_{44}}{s_{14}}, & \lambda_8 = \dfrac{s_{12}s_{44}}{s_{14}}, & \lambda_9 = \dfrac{s_{43}s_{14} - s_{13}s_{44}}{s_{14}}, \end{cases} \tag{20}$$

in which the parameters $s_{k_{\mathrm{w}}}$, $s_{k_{\mathrm{p}}}$, and $s_{T_{\mathrm{H}}}$ are defined as

$$\begin{cases} s_{k_{\mathrm{w}}} = \dfrac{\delta_1^2(\mathrm{e}^{-2(\eta+1)x_0}-1)}{4((\eta+1)^2+\delta_1^2)(\eta+1)}, \\ s_{k_{\mathrm{p}}} = \dfrac{\delta_1^2\left(\mathrm{e}^{-2\eta x_0}-1\right)\left(\eta^2+\delta_1^2+\delta_2^2\right)}{4\left(\eta^2+\delta_1^2\right)\eta x_2^2}, \\ s_{T_{\mathrm{H}}} = \dfrac{(2\delta_1^2+2\eta^2+2\eta+1+4\delta_2^2)\delta_1^2(\mathrm{e}^{(2\eta+1)x_0}-1)}{2x_2(1+2\eta)((1+2\eta)^2+4\delta_1^2)\cot\theta}. \end{cases} \tag{21}$$

When $k_2 = 0$ is taken into account in Eq. (19), the expression for the DHBP of TCSs reinforced with CNTs on the W-EF within the FOSDT is obtained and the symbol $T_{1\mathrm{sdt}}^{\mathrm{crw}}$ is used.

When $k_1 = k_2 = 0$ are taken into account, the expression for the DHBP ($T_{1\mathrm{sdt}}^{\mathrm{cr}}$) of TCSs reinforced with CNTs without EFs on the basis of the FOSDT is obtained.

Since the influence of shear stresses is ignored from Eq. (19), the expressions for the HBP of TCSs reinforced with CNTs on the W- and P-EFs within the CST are found and the symbols $T_{1\mathrm{cst}}^{\mathrm{crwp}}$ and $T_{1\mathrm{cst}}^{\mathrm{crw}}$ are used.

Finding the magnitudes of the DHFP for TCSs reinforced by CNTs on the EFs within FOSDT is achieved by minimizing Eq. (19) in accordance with the number of circumferential waves for different η. Various numerical calculations and analyzes show that the magnitudes of the DHBP for F-S TCSs reinforced by CNTs are obtained at $\eta = 2.4$.

4 Numerical results and discussion

4.1 Key specifications of TCSs reinforced with CNTs

In this part, key specifications of TCSs reinforced with CNTs are defined. Poly (methyl methacrylate), referred to as PMMA, is selected for the matrix with material properties $Y^{\mathrm{m}} = 2.5$ Pa, $p^{\mathrm{m}} = 0.34$, $d^{\mathrm{m}} = 1\ 150\ \mathrm{kg/m}^3$, and (10,10) armchair SWCNT with length $\widetilde{L} = 9.26$ nm, radius $\widetilde{r} = 0.68$ nm, and thickness $\widetilde{h} = 0.067$ nm is chosen as the reinforcements.

Three different types of TCSs reinforced with CNTs, namely, uniformly distribution (UD), i.e., $V_{\mathrm{cn}} = V_{\mathrm{cn}}^*$, linear distributions across the TCS thickness in the form (VD) and (XD) are used and are expressed as $V_{\mathrm{cn}} = \left(1 - 2\overline{\zeta}\right) V_{\mathrm{cn}}^*$ and $V_{\mathrm{cn}} = 4\left|\overline{\zeta}\right| V_{\mathrm{cn}}^*$, respectively[9–12].

The topologies of the cross-section of UD, VD, and XD-TCSs are depicted in Fig. 2.

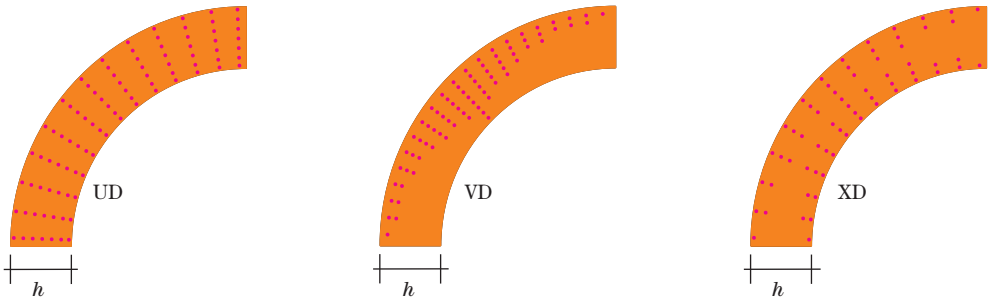

Fig. 2 The topologies of TCSs reinforced with CNTs (color online)

Typical values of the effective material properties of the TCSs reinforced with CNTs are calculated at $T = 300$ K as follows[12]:

$$Y_{11}^{\rm cn} = 6.183\ 87 - 0.002\ 86T + 4.228\ 67 \times 10^{-6}T^2 - 2.272\ 4 \times 10^{-9}T^3 = 5.646\ 6\,\text{TPa},$$
$$Y_{22}^{\rm cn} = 7.753\ 48 - 0.003\ 58T + 5.300\ 57 \times 10^{-6}T^2 - 2.848\ 68 \times 10^{-9}T^3 = 7.080\ 0\,\text{TPa},$$
$$S_{12}^{\rm cn} = 1.801\ 26 + 7.784\ 5 \times 10^{-4}T - 1.127\ 9 \times 10^{-6}T^2 + 4.934\ 84 \times 10^{-10}T^3 = 1.944\ 5\,\text{TPa},$$
$$p_{12}^{\rm cn} = 0.175, \quad d^{\rm cn} = 1\ 400\,\text{kg/m}^3.$$

The efficiency parameters for different volume fractions of CNTs are[13]

$$e_1 = 0.137, \quad e_2 = 1.022, \quad e_3 = 0.715 \quad \text{for} \quad V_{\rm cn}^* = 0.12;$$
$$e_1 = 0.142, \quad e_2 = 1.626, \quad e_3 = 1.138 \quad \text{for} \quad V_{\rm cn}^* = 0.17;$$
$$e_1 = 0.141, \quad e_2 = 1.585, \quad e_3 = 1.109 \quad \text{for} \quad V_{\rm cn}^* = 0.28.$$

These key properties are used in the next subheadings.

4.2 Comparison

In this subheading, numerical comparisons are made to prove the formula (19) obtained for the DHBP of TCSs reinforced with CNTs under F-S boundary conditions within the FOSDT and are presented in Tables 1−3. Since the buckling problem of TCSs reinforced with CNTs within the FOSDT under the UHP and resting on the EFs has not yet been solved, our results are compared with the HBP for homogeneous isotropic shells and with the lateral buckling pressure for TCSs reinforced with CNTs without EFs in the framework of the FOSDT.

In Table 1, the magnitudes of DHBP of metal TCSs within the CST are compared with the results of Ref. [34]. In the computation of Eq. (19), we take into account $V_{\rm cn}^* = 0$, $V_{\rm m} = 1$, $k_1 = k_2 = 0$, $E_{11} = E_{22} = E_{\rm m}$, and $\nu_{12} = \nu_{\rm m}$. The data were adopted as[34] $E_{\rm m} = 2.1 \times 10^{11}$ (N/m^2), $\nu_{\rm m} = 0.3$ and $h/r_1 = 1/100$; $r_1/l = 0.5$; $r_1/l = 2.0$. The values in parentheses are the buckling mode corresponding to the HBP. It is seen from Table 1 that the values of dimensionless DHBP are in good agreement with the results of Ref. [34].

Table 1 Comparison of the values of DHBPs of metal TCSs in the framework of the CST

θ	$T_{1\rm cst}^{\rm cr} \times 10^6 (n_{\rm cr})$			
	$r_1/l = 0.5$		$r_1/l = 2$	
	Ref. [34]	Present study	Ref. [34]	Present study
10°	3.74 (7)	3.70 (7)	19.40 (11)	19.39 (11)
30°	2.23 (8)	2.15 (8)	14.55 (11)	14.51 (11)
50°	1.16 (8)	1.14 (9)	8.81 (11)	8.73 (11)

In Table 2, the lateral buckling pressure (LBP), unconstrained TCSs reinforced with CNTs, are compared with the results of Ref. [35]. This comparison uses features of the TCS reinforced by CNTs, as described in the previous subheading. The specific properties of the cone are listed as follows: $l = 0.017\ 32$, $r_1 = 0.1$, $h = 0.001$ m. From Table 2 it can be seen that the LBP for TCSs reinforced with CNTs are in good agreement with the results of Ref. [35] which is used the GDQ method. The values in parentheses indicate the buckling mode.

Table 2 Comparison of the LBP (kPa) and buckling mode for TCSs reinforced with different CNTs in the framework of FOSDT without the EFs

θ	$V_{\rm cn}^*$	Present study		Ref. [35]	
		UD	VD	UD	VD
30°	0.12	11.494 (10)	11.863 (10)	11.47 (10)	11.69 (10)
	0.17	19.057 (10)	19.767 (10)	19.00 (9)	19.53 (10)
	0.28	22.335 (10)	23.014 (10)	22.30 (10)	23.10 (10)
40°	0.12	8.529 (10)	8.739 (10)	8.61 (10)	8.710 (10)
	0.17	14.094 (10)	14.526 (10)	14.22 (10)	14.51 (10)
	0.28	16.669 (10)	16.973 (10)	16.85 (10)	17.26 (10)

The values of HBP (ψ) of metal TCSs in the framework of the FOSDT without EFs are compared with the higher order shear deformation theory (HOSDT) results obtained in Ref. [36]. When the data $V_{\rm cn}^{*}=0$, $V_{\rm m}=1$, $k_1=k_2=0$, $E_{11}=E_{22}=E_{\rm m}$, $\nu_{12}=\nu_{\rm m}$ and $\theta\to 0^{\circ}$ are taken into account in Eq. (19), it is expressed for the HBP of pure metal cylindrical shells in the framework of FOSDT. The calculations are performed using these data for various Batdorf parameter $Z_{\rm B}$, and the numerical results are presented in Table 3 together with the magnitudes of HBPs in the framework of HOSDT in the study of Shen and Noda[36]. Since the minimum HBP values of cylindrical shells are independent of the parameter η, therefore, $\eta=0$ is taken into account in the calculations. The material and shell parameters are used[36]: $E_{\rm m}=10^7$ (ψ), $\nu_{\rm m}=0.33$ and $h=1$ inc, $h/r=1/50$, $l_1=(Z_{\rm B}rh/(1-\nu_{\rm m}^2)^{0.5})^{0.5}$. Here l_1 is the length of the cylindrical shell. The values in brackets indicate the buckling mode. Table 3 shows that the HBP values of cylindrical shells in our results agree very well with existing results.

Table 3 Comparison of the values of HBP (ψ) of metal cylindrical shells within FOSDT

$Z_{\rm B}$	50	100	500	1 000	5 000	10 000
Ref. [36] (HOSDT)	566.09 (7)	389.62 (6)	166.77 (4)	124.98 (3)	56.5 (2)	37.02 (4)
Present study (FOSDT)	566.75 (7)	389.92 (6)	166.81 (4)	124.997 (3)	56.57 (2)	37.02 (4)

4.3 New analysis of TCSs reinforced with CNTs on the EFs

The HBPs for UD, VD, and XD-TCSs resting on the P-EF and without ground in the framework of FOSDT and CST are compared according to the variation of the half-peak angle θ (see Table 4 and Figs. 3–5). The data in Table 4 are calculated numerically from formula (19) using the following TCS and EF parameters: $l/r_1=0.5, h/r_1=1/25$, $(k_{\rm w},k_{\rm p})=(0,0)$ and $(k_{\rm w},k_{\rm p})=(8\times 10^8\,{\rm N/m^3},\ 4\times 10^4\ {\rm N/m})$. Two different volume fractions $V_{\rm cn}^{*}=0.17$ and 0.28 are used in the calculations. The curves in Figs. 3–5 are plotted using the values from Table 4. As can be seen, although the magnitudes of the HBP for each θ within the FOSDT are lower than the magnitudes within the CST, the presence of the elastic foundation affects the magnitudes of the buckling pressure in both shell theories in the direction of their increase (see Figs. 3–4).

The buckling mode increases with the increasing of the half-peak angle θ, and also it increases considering the influence of the P-EF. The smallest buckling mode corresponding to the HBP occurs in the VD-TCS. As the linear distribution of CNTs in the matrix is in the form of VD, the influence of heterogeneity on the DHBP is significantly lower than that the distribution in the form of XD. An increase of the θ apparently reduces the influence of inhomogeneity on the DHBP for the TCS with the XD-type distribution of CNTs faster than the VD-type distribution of CNTs within the FOSDT (see Fig. 5). For example; although the influence of heterogeneity on the $T_{\rm 1sdt}^{\rm crwp}$ decreases from (-2.69%) to (-1.23%) for the VD-type distribution of CNTs, this effect decreases from ($+8.42\%$) to ($+1.05\%$) for the XD-type distribution of CNTs, as the θ increases from 15° to 75° for $V_{\rm cn}^{*}$=0.17 (see Table 4). For these data, the heterogeneity is more effective around 2%, when the P-EF is not taken into account. Furthermore, in the XD-type distribution of CNTs, the heterogeneity is more effective at $V_{\rm cn}^{*}$=0.17 than the case $V_{\rm cn}^{*}$=0.28, but reverses for the VD distribution of CNTs. Consideration of the P-EF reduces the apparent shear strains on the $T_{\rm 1sdt}^{\rm crwp}$ around 5%. The influence of the P-EF on the values of the buckling load increases 10% within FOSDT, as the θ increases from 15° to 75°. In addition, influence of the P-EF is found to be about 11%–18% more prominent within the FOSDT than the CST.

Table 4 Comparison of the magnitudes of T_1^{crwp} and T_1^{cr} for the UD, VD, and XD-TCSs within the FOSDT and CST

$\theta/(^\circ)$	Type	$T_{1\mathrm{sdt}}^{\mathrm{crwp}} \times 10^3$ $(k_{\mathrm{w}}, k_{\mathrm{p}}) = (0, 0)$	$T_{1\mathrm{cst}}^{\mathrm{crwp}} \times 10^3$ $(k_{\mathrm{w}}, k_{\mathrm{p}}) = (0, 0)$	$T_{1\mathrm{sdt}}^{\mathrm{crwp}} \times 10^3$ $(k_{\mathrm{w}}, k_{\mathrm{p}}) = (4 \times 10^9\ \mathrm{N/m^3}, 3 \times 10^4\ \mathrm{N/m})$	$T_{1\mathrm{cst}}^{\mathrm{crwp}} \times 10^3$ $(k_{\mathrm{w}}, k_{\mathrm{p}}) = (4 \times 10^9\ \mathrm{N/m^3}, 3 \times 10^4\ \mathrm{N/m})$
		$V_{\mathrm{cn}}^* = 0.17$			
	UD	2.665 (14)	4.193 (15)	3.276 (15)	4.762 (15)
15	VD	2.538 (13)	3.588 (13)	3.188 (14)	4.229 (14)
	XD	2.956 (14)	5.353 (16)	3.552 (15)	5.883 (16)
	UD	1.999 (14)	3.500 (15)	2.514 (16)	3.987 (16)
30	VD	1.914 (14)	2.992 (14)	2.458 (15)	3.542 (15)
	XD	2.165 (15)	4.477 (17)	2.666 (16)	4.924 (17)
	UD	1.406 (15)	2.679 (16)	1.806 (16)	3.066 (17)
45	VD	1.352 (14)	2.284 (14)	1.775 (16)	2.718 (15)
	XD	1.491 (16)	3.427 (17)	1.879 (17)	3.784 (18)
	UD	0.891 (16)	1.801 (16)	1.162 (17)	2.067 (17)
60	VD	0.858 (15)	1.532 (14)	1.146 (16)	1.833 (16)
	XD	0.926 (16)	2.307 (18)	1.190 (17)	2.551 (18)
	UD	0.431 (16)	0.903 (16)	0.569 (17)	1.039 (17)
75	VD	0.415 (15)	0.765 (15)	0.562 (17)	0.918 (16)
	XD	0.442 (17)	1.156 (18)	0.575 (18)	1.283 (18)
$\theta/(^\circ)$		$V_{\mathrm{cn}}^* = 0.28$			
	UD	3.276 (15)	4.762 (15)	3.797 (15)	6.110 (17)
15	VD	3.188 (14)	4.229 (14)	3.740 (14)	5.395 (15)
	XD	3.552 (15)	5.883 (16)	4.230 (15)	8.149 (17)
	UD	2.514 (16)	3.987 (16)	2.882 (16)	5.119 (17)
30	VD	2.458 (15)	3.542 (15)	2.846 (15)	4.518 (16)
	XD	2.666 (16)	4.924 (17)	3.120 (16)	6.820 (18)
	UD	1.806 (16)	3.066 (17)	2.050 (17)	3.929 (18)
45	VD	1.775 (16)	2.718 (15)	2.029 (16)	3.468 (16)
	XD	1.879 (17)	3.784 (18)	2.161 (17)	5.239 (19)
	UD	1.162 (17)	2.067 (17)	1.310 (18)	2.651 (19)
60°	VD	1.146 (16)	1.833 (16)	1.299 (17)	2.336 (17)
	XD	1.190 (17)	2.551 (18)	1.347 (17)	3.530 (19)
	UD	0.569 (17)	1.039 (17)	0.637 (18)	1.330 (19)
75	VD	0.562 (17)	0.918 (16)	0.633 (17)	1.171 (17)
	XD	0.575 (18)	1.283 (18)	0.646 (18)	1.774 (20)

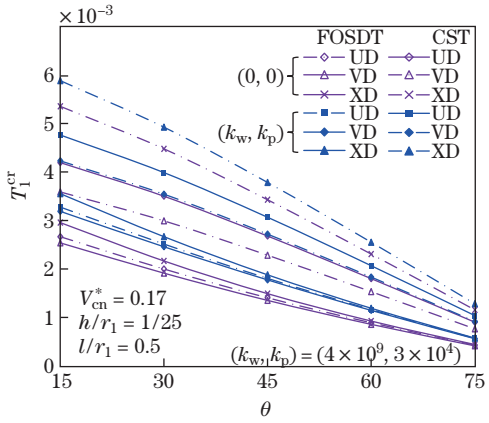

Fig. 3 Variations of HBPs for UD, VD, and XD-TCSs with and without P-EF versus θ for $V_{\mathrm{cn}}^* = 0.17$ (color online)

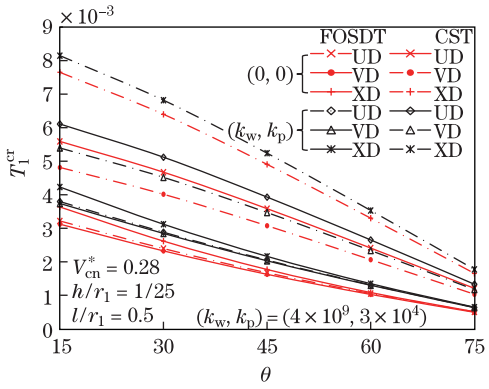

Fig. 4 Variations of HBPs for UD, VD, and XD-TCSs with and without P-EF versus θ for $V_{\rm cn}^{*} = 0.28$ (color online)

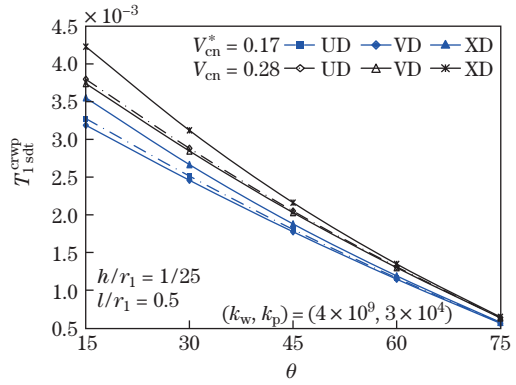

Fig. 5 Variations of HBPs for UD, VD, and XD-TCSs with and without P-EF on the basis of the FOSDT versus the θ for $V_{\rm cn}^{*} = 0.17$ and 0.28 (color online)

In Fig. 6, the curves of $T_{1\rm sdt}^{\rm crwp}$ and $T_{1\rm cst}^{\rm crwp}$ for UD and VD-TCSs on the W-EF and P-EF are shown in accordance with the r_1/h ratio and compared with the corresponding curves of the same TCSs without EFs. The parameters of the TCS and EFs which are used to construct the curves in Fig. 6 as follows: $r_1/l = 2, \theta = 30^{\circ}, V_{\rm cn}^{*} = 0.12$, $(k_{\rm w}, k_{\rm p}) = (0,0); (8\times10^{8}, 0); (8\times10^{8}; 4\times10^{4})$. The buckling pressures of UD and VD-TCSs on the W-EF and P-EF decrease due to an increase of the r_1/h ratio. The influence of the linear distribution of CNTs in the form of VD on the DHBP weakens more if the TCS relies on the P-EF than relies on the W-EF. In addition, as the small radius to thickness ratio increases, the influences of W-EF and P-EF on the hydrostatic buckling loads for UD and VD-TCSs increase. The influence of shear strains on the DHBPs is more pronounced, if the TCS is on the W-EF than on the P-EF and it reduces, as the r_1/h increases. For instance, the influences of shear stresses on the DHBPs of VD-TCSs on the W- and P-EFs decrease from 37.47% to 11.5% and 32.86% to 9.02%, respectively, when the r_1/h ratio increases from 25 to 40. In addition to the fact that the difference between the influences of P-EF and W-EF on the HBPs is significant, it is determined that this difference increases significantly with increasing the r_1/h ratio.

The curves defining the change of buckling pressures for UD, VD, and XD-TCSs on W-EF and P-EF are plotted using different theories in Fig. 7 depending on the change of l/r_1. The data used for the drawing of Fig. 7 are considered as follows: $h/r_1 = 1/25$, $\theta = 30^{\circ}$, $V_{\rm cn}^{*} = 0.12$, $(k_{\rm w}, k_{\rm p}) = (0,0)$; $(4.5\times10^{8}, 0)$; $(4.5\times10^{8}; 1.5\times10^{4})$. As can be seen from Fig. 7, considering the effects of P-EF and W-EF on the buckling pressures of the UD, VD, and XD- TCSs, their

rate of decrease is weakened due to the increase of the l/r_1 ratio. As l/r_1 increases from 0.6 to 1, the influences of soils on the buckling loads of UD, VD, and XD-TCSs increase significantly, and the influences of W-EF and P-EF on the buckling loads of VD-TCSs with length l/r_1 make up (+25.6%) and (+46.86%), respectively. An increase of the l/r_1 ratio reduces the influence of shear stresses on the buckling loads, and the effects of EFs further reduce the influence of shear stresses.

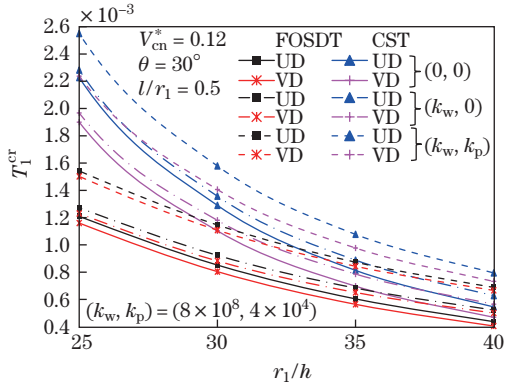

Fig. 6 Variations of DHBPs for UD, VD, and XD- TCSs on the W-EF and P-EF within two theories versus r_1/h (color online)

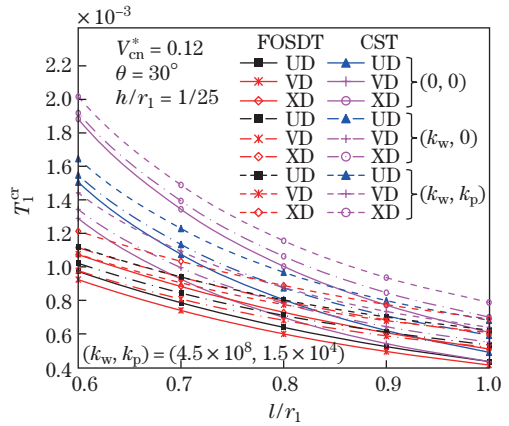

Fig. 7 Variations of DHBPs for UD, VD, and XD- TCSs on the W-EF and P-EF within two theories versus l/r_1 (color online)

5 Conclusions

In this study, the effects of W-EF, P-EF, and CNT reinforcement on the DHBP for the TCSs are investigated. The material properties of TCSs reinforced with CNTs are graded linearly according to the thickness coordinate. The basic relations and equations of TCSs reinforced with CNTs on the EFs are obtained in the framework of the FOSDT and solved using the Galerkin method. The novelty of this study is to obtain closed-form solutions for the HBP of TCSs reinforced with CNTs on the EFs. Finally, the effects of the EFs and various types CNT reinforcements on the DHBP are investigated simultaneously. The obtained results are compared with the results in the literature, and the accuracy of present results is confirmed.

References

[1] LIM, H. E., MIYATA, Y., KITAURA, R., NISHIMURA, Y., NISHIMOTO, Y., IRLE, S., WARNER, J. H., KATAURA, H., and SHINOHARA, H. Growth of carbon nanotubes via twisted graphene nanoribbons. *Nature Communications*, **4**, 2548 (2013)

[2] ALIZADA, A. N., SOFIYEV, A. H., and KURUOGLU, N. The stress analysis of the substrate coated by nanomaterials with vacancies subjected to the uniform extension load. *Acta Mechanica*, **223**, 1371–1383 (2012)

[3] POWER, A. C., GOREY, B., CHANDRA, S., and CHAPMAN, J. Carbon nanomaterials and their application to electrochemical sensors: a review. *Nanotechnology Reviews*, **7**(1), 19–41 (2018)

[4] PASTERNAK, P. L. *On a New Method of Analysis of an Elastic Foundation by Means of Two Foundation Constants*, State Publishing House of Literature on Construction and Architecture, Moscow, 1–56 (1954)

[5] KERR, A. D. Elastic and viscoelastic foundation models. *ASME Journal of Applied Mechanics*, **31**, 491–498 (1964)

[6] BAJENOV, V. A. *The Bending of the Cylindrical Shells in an Elastic Medium*, Visha Shkola Publishing House, Kiev (1975)

[7] SHENG, G. G. and WANG, X. Thermal vibration, buckling and dynamic stability of functionally graded cylindrical shells embedded in an elastic medium. *Journal of Reinforced Plastics and Composites*, **27**(2), 117–134 (2008)

[8] SUN, B. and HUANG, Y. The exact solution for the general bending problems of conical shells on the elastic foundation. *Applied Mathematics and Mechanics* (*English Edition*), **9**(5), 455–469 (1988) https://doi.org/10.1007/BF02465684

[9] SHEN, H. S. and XIANG, Y. Postbuckling of axially compressed nanotube-reinforced composite cylindrical panels resting on elastic foundations in thermal environments. *Composites Part B*: *Engineering*, **67**, 50–61 (2014)

[10] SHEN, H. S. and XIANG, Y. Nonlinear bending of nanotube-reinforced composite cylindrical panels resting on elastic foundations in thermal environments. *Engineering Structures*, **80**, 163–172 (2014)

[11] SHEN, H. S. and XIANG, Y. Nonlinear vibration of nanotube-reinforced composite cylindrical panels resting on elastic foundations in thermal environments. *Composite Structures*, **111**, 291–300 (2014)

[12] SHEN, H. S. and XIANG, Y. Nonlinear response of nanotube-reinforced composite cylindrical panels subjected to combined loadings and resting on elastic foundations. *Composite Structures*, **131**, 939–950 (2015)

[13] SHEN, H. S. and XIANG, Y. Thermal postbuckling of nanotube-reinforced composite cylindrical panels resting on elastic foundations. *Composite Structures*, **123**, 383–392 (2015)

[14] BIDGOLI, M. R., KARIMI, M. S., and ARANI, A. G. Nonlinear vibration and instability analysis of functionally graded CNT-reinforced cylindrical shells conveying viscous fluid resting on orthotropic Pasternak medium. *Mechanics of Advanced Materials and Structures*, **23**(7), 819–831 (2016)

[15] MOHAMMADI, M., AREFI, M., DIMITRI, R., and TORNABENE, F. Higher-order thermo-elastic analysis of FG-CNTRC cylindrical vessels surrounded by a Pasternak foundation. *Nanomaterials*, **9**(1), 79 (2019)

[16] SHEN, H. S. and ZHU, Z. H. Postbuckling of sandwich plates with nanotube-reinforced composite face sheets resting on elastic foundations. *European Journal of Mechanics-A/Solids*, **35**, 10–21 (2012)

[17] ALIBEIGLOO, A. Three-dimensional free vibration analysis of multi-layered graphene sheets embedded in elastic matrix. *Journal of Vibration and Control*, **19**(16), 2357–2371 (2013)

[18] SHABAN, M. and ALIBEIGLOO, A. Three-dimensional vibration and bending analysis of carbon nanotubes embedded in elastic medium based on theory of elasticity. *Latin American Journal of Solids and Structures*, **11**(12), 2122–2140 (2014)

[19] ZHANG, L. W., LEI, Z., and LIEW, K. M. Computation of vibration solution for functionally graded carbon nanotube-reinforced composite thick plates resting on elastic foundations using the element-free IMLS-Ritz method. *Applied Mathematics and Computation*, **256**, 488–504 (2015)

[20] ZHANG, L. W., SONG, Z. G., and LIEW, K. M. Nonlinear bending analysis of FG-CNT reinforced composite thick plates resting on Pasternak foundations using the element-free IMLS-Ritz method. *Composite Structures*, **128**, 165–175 (2015)

[21] ZHANG, L. W. and LIEW, K. M. Postbuckling analysis of axially compressed CNT reinforced functionally graded composite plates resting on Pasternak foundations using an element-free approach. *Composite Structures*, **138**, 40–51 (2016)

[22] FU, Y., ZHONG, J., SHAO, X., and TAO, C. Analysis of nonlinear dynamic stability for carbon nanotube-reinforced composite plates resting on elastic foundations. *Mechanics of Advanced Materials and Structures*, **23**(11), 1284–1289 (2016)

[23] SHEN, H. S., XIANG, Y., and LIN, F. Nonlinear bending of functionally graded graphene-reinforced composite laminated plates resting on elastic foundations in thermal environments. *Composite Structures*, **170**, 80–90 (2017)

[24] GOLMAKANI, M. E. and ZEIGHAMI, V. Nonlinear thermo-elastic bending of functionally graded carbon nanotube-reinforced composite plates resting on elastic foundations by dynamic relaxation method. *Mechanics of Advanced Materials and Structures*, **25**(10), 868–880 (2018)

[25] GAO, K., GAO, W., CHEN, D., and YANG, J. Nonlinear free vibration of functionally graded graphene platelets reinforced porous nanocomposite plates resting on elastic foundation. *Composite Structures*, **204**, 831–846 (2018)

[26] DUC, N. D., LEE, J., NGUYEN-THOI, T., and THANG, P. T. Static response and free vibration of functionally graded carbon nanotube-reinforced composite rectangular plates resting on Winkler-Pasternak elastic foundations. *Aerospace Science and Technology*, **68**, 391–402 (2017)

[27] KELESHTERI, M. M., ASADI, H., and AGHDAM, M. M. Nonlinear bending analysis of FG-CNTRC annular plates with variable thickness on elastic foundation. *Thin-Walled Structures*, **135**, 453–462 (2019)

[28] DUC, N. D., CONG, P. H., TUAN, N. D., TRAN, P., and THANH, N. V. Thermal and mechanical stability of functionally graded carbon nanotubes (FG CNT)-reinforced composite truncated conical shells surrounded by the elastic foundations. *Thin-Walled Structures*, **115**, 300–310 (2017)

[29] THANH, N. V., QUANG, V. D., KHOA, N. D., EOCK, K. S., and DUC, N. D. Nonlinear dynamic response and vibration of FG CNTRC shear deformable circular cylindrical shell with temperature-dependent material properties and surrounded on elastic foundations. *Journal of Sandwich Structures & Materials*, **21**(7), 2456–2483 (2019)

[30] AMBARTSUMIAN, S. A. *Theory of Anisotropic Shells*, State Publishing House for Physical and Mathematical Literature, Moscow (1961)

[31] VOLMIR, A. S. *Stability of Elastic Systems*, Nauka, Moscow (1967)

[32] ESLAMI, M. R. *Buckling and Postbuckling of Beams*, *Plates and Shells*, Springer, Switzerland (2018)

[33] SOFIYEV, A. H., TURKASLAN-ESENCAN, B., BAYRAMOV, R. P., and SALAMCI, M. U. Analytical solution of stability of FG-CNTRC conical shells under external pressures. *Thin-Walled Structures*, **144**, 1–12 (2019)

[34] BARUCH, M., HARARI, O., and SINGER, J. Influence of in-plane boundary conditions on the stability of conical shells under hydrostatic pressure. *Israel Journal of Technology*, **5**, 12–24 (1967)

[35] JAM, J. E. and KIANI, Y. Buckling of pressurized functionally graded carbon nanotube reinforced conical shells. *Composite Structures*, **125**, 586–595 (2015)

[36] SHEN, H. S. and NODA, N. Post-buckling of pressure-loaded FGM hybrid cylindrical shell in thermal environments. *Composite Structures*, **77**, 546–560 (2007)